# Supporting Information

## Experimental section

### Materials

Molybdenum sulfide ($MoS_2$) powder was purchased from Shanghai Aladdin Biochemical Technology Co., Ltd. Tungsten disulfide ($WS_2$) powder was purchased from Nanjing Xianfeng Nano Material Technology Co., Ltd. Adenosine, adenosine diphosphate (ADP), adenosine triphosphate (ATP), uridine, guanosine, thymidine and cytidine were purchased from Bioengineering (Shanghai) Co., Ltd. carboxyfluorescein (FAM)-labelled anti-adenosine aptamer (5'- FAM- AAC CTG GGG GAG TAT TGC GGA GGA AGGT- 3') were synthesized and purified by Sangon Biotech (Shanghai) Co., Ltd. Other chemicals were used as received without further purification. All experimental water used was ultrapure water (18.2 MΩ CM, Millipore).

### Preparation of $MoS_2$ nanosheets

Experimentally, 200 mg $MoS_2$ powder was added into 40 mL aqueous solution containing 40 mg ATP. The mixed suspension was ultrasonic exfoliation for 30 h. After centrifugation at 6000 rpm for 20 min to remove large particles, the supernatant was collected. The collected supernatant was further centrifuged at 12000 rpm for 10 min, the supernatant was removed, and the sediment was re-dispersed in water. Similarly, ADP and adenosine were used to prepare $MoS_2$ nanosheets under the same procedure respectively. In addition, ATP was also used to exfoliate $WS_2$ powder by the same method.

### Characterization

Transmission electron microscopy (TEM) image, selected area electron diffraction (SAED) pattern and high-resolution TEM image of as-exfoliated $MoS_2$ nanosheets were characterized by an FEI Tecnai G2F20 transmission electron microscope with the accelerating voltage of 200 kV. Before measurement, the dispersion of as-exfoliated $MoS_2$ nanosheets was diluted with ethanol, dropped onto the carbon film supported by the copper mesh, and naturally dried by air. Atomic

force microscopy (AFM) image of as-exfoliated $MoS_2$ nanosheets was characterized by a Bruker Multimode III scanning probe microscope. Before measurement, the dispersion solution of as-exfoliated $MoS_2$ nanosheets was diluted with ethanol, dropped onto the mica plate and dried by $N_2$. X-ray photon spectroscopy (XPS) spectra of $MoS_2$ nanosheets were characterized by a Thermo Scientific ESCALAB 250 X-ray photoelectron spectrometer. Before measurement, the dispersion solution of as-exfoliated $MoS_2$ nanosheets was concentrated by centrifugation, and then added dropwisely to the surface of the silicon wafer and air-dried. The X-ray diffraction (XRD) pattern of $MoS_2$ nanosheets was measured by an Ultima IV X-ray diffractometer. Before measurement, the dispersion solution of $MoS_2$ nanosheets was concentrated by centrifugation, dropped into the groove of a glass slide, and air-dried until the groove of the glass slide was filled with a thin layer of $MoS_2$ nanosheets. The particle size distribution and zeta potential of $MoS_2$ nanosheets were measured by dynamic light scattering (DLS) by using a Malvern zetasize nano-zs90 nanoparticle size potential analyzer. Before measurement, the dispersion solution of $MoS_2$ nanosheets was diluted with water.

**Fluorescent biosensor for adenosine**

40 μL FAM-labelled anti-adenosine aptamer (100 nmol $L^{-1}$) was mixed with 325 μL different concentrations of adenosine in Tris-HCl buffer (20 mmol $L^{-1}$, pH 7.4, 100 mmol $L^{-1}$ NaCl, 5 mmol $L^{-1}$ KCl, 5 mmol $L^{-1}$ $MgCl_2$). The mixture was incubated in a metal bath at 25 °C for 20 min with a slight shaking (300 rpm). Then, 35 μL dispersion solution of $MoS_2$ nanosheets (0.24 mg $mL^{-1}$) was added，the mixture was further incubated for 5 min in a metal bath at 25 °C with a slight shaking (300 rpm). Finally, the fluorescent spectrum was recorded by a F4600 fluorospectrometer.

The pretreatment for human serum samples was as follows: 50 μL serum sample was mixed with 500 μL $Ba(OH)_2$ solution (0.08 mmol $L^{-1}$) and 500 μL $ZnSO_4$ solution (0.10 mmol $L^{-1}$), followed by vortexing for 10 s; the mixture was centrifuged at 8000 rpm for 10 min, and the supernatant was 10-fold diluted with tris-HCl buffer (20 mmol $L^{-1}$, pH 7.4, 100 mmol $L^{-1}$ NaCl, 5 mmol $L^{-1}$ KCl, 5 mmol $L^{-1}$ $MgCl_2$) and spiked with different concentration of adenosine.

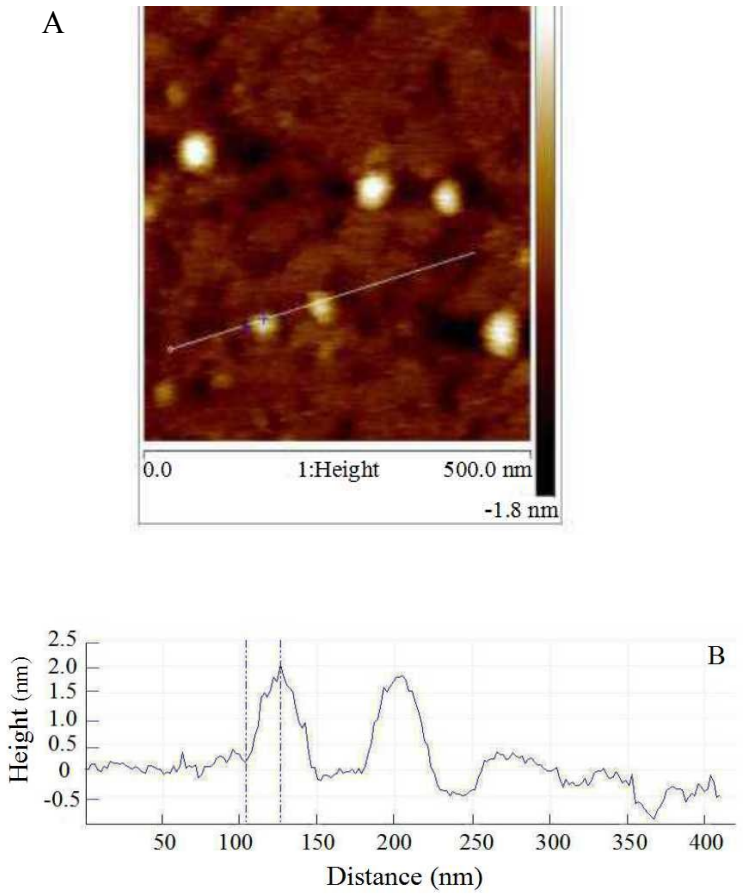


**Figure S1.** AFM image (A) and height profile (B) of as-exfoliated $MoS_2$ nanosheets

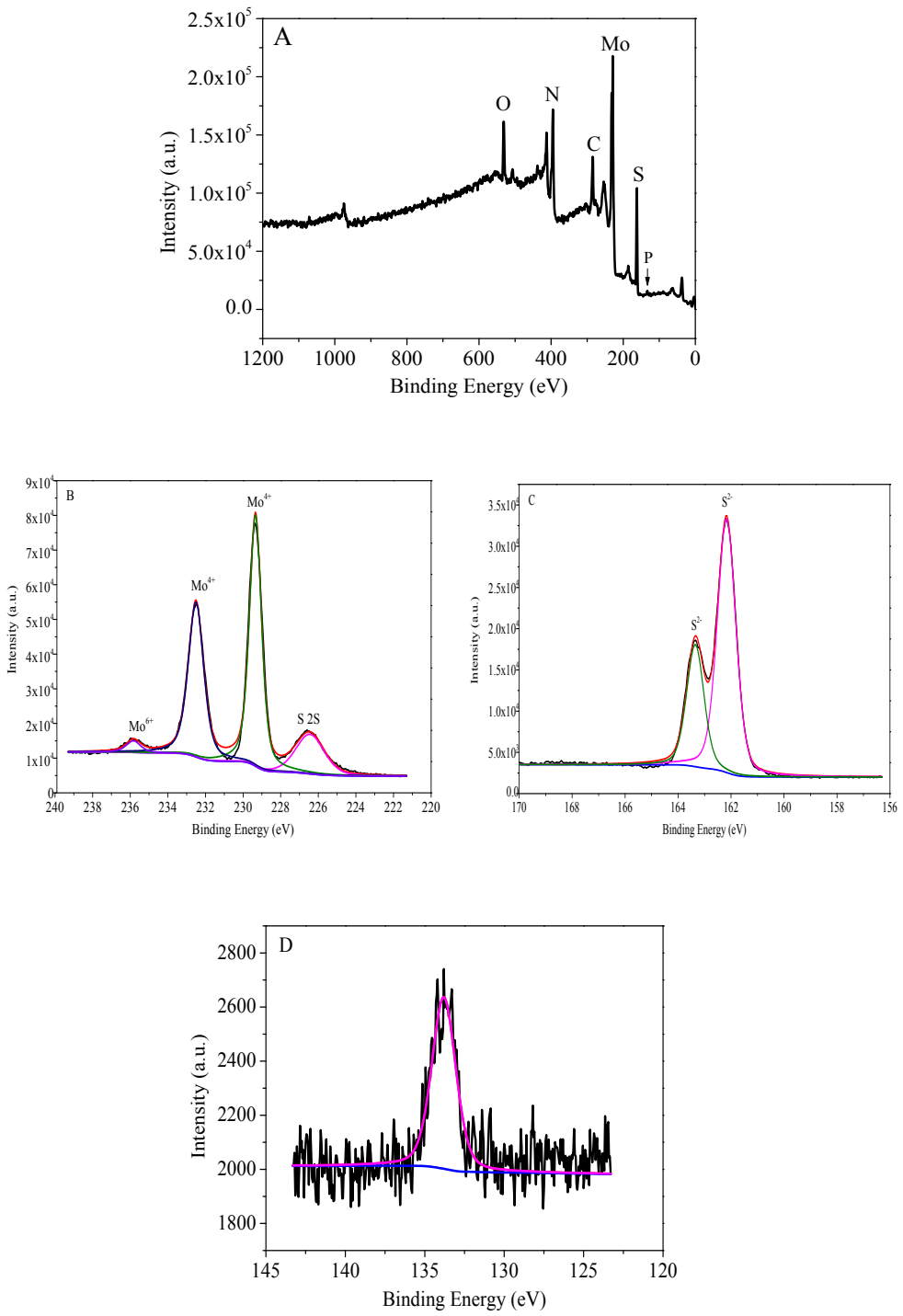


**Figure S2.** The survey XPS spectrum (A), Mo 3d (B), S 2P (C) and P 2P (D) core-level XPS of as-exfoliated $MoS_2$ nanosheets.

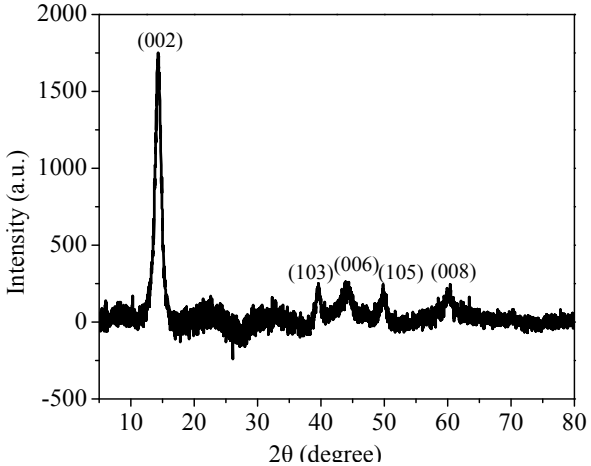


**Figure S3.** XRD pattern of as-exfoliated $MoS_2$ nanosheets

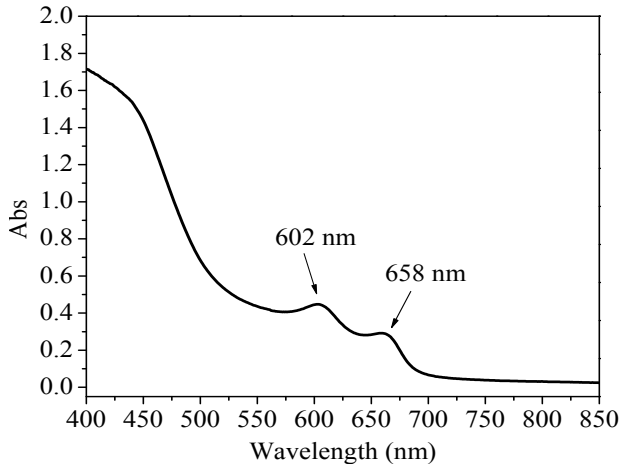


**Figure S4.** Absorption spectrum of dispersion solution of as-exfoliated $MoS_2$ nanosheets (0.28 mg $mL^{-1}$)

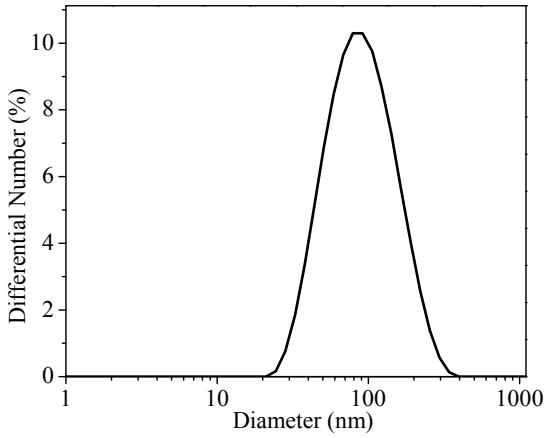


**Figure S5.** The size distribution of as-exfoliated $MoS_2$ nanosheets

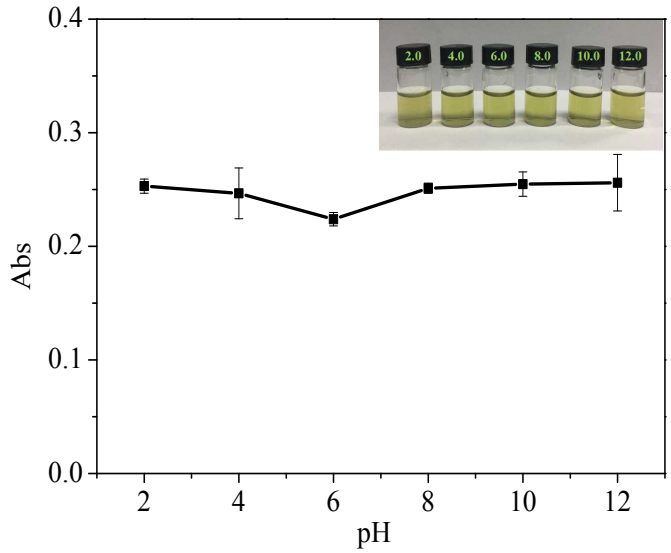


**Figure S6.** Absorption intensities at 658 nm of as-exfoliated $MoS_2$ nanosheets (0.2 mg $mL^{-1}$) in various pH phosphate buffer (10 mmol $L^{-1}$). Insert were the corresponding photos of as-exfoliated $MoS_2$ nanosheets in pH 2.0, pH 4.0, pH 6.0, pH 8.0, pH 10.0 and pH 12.0 phosphate buffers (10 mmol $L^{-1}$).

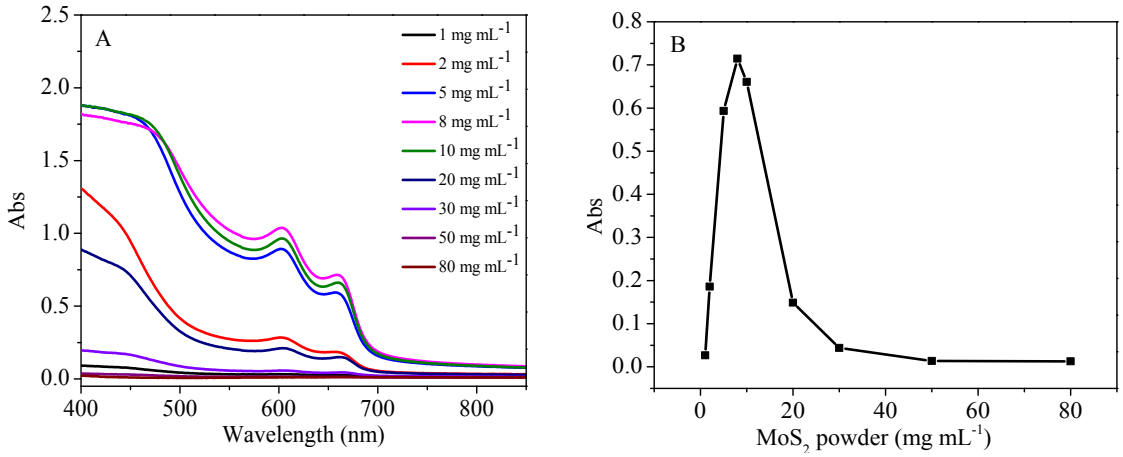


**Figure S7.** Absorption spectra of as-exfoliated $MoS_2$ nanosheets with different mass concentration of $MoS_2$ powder (A) and the relationship between absorption intensity of as-exfoliated $MoS_2$ nanosheets at 658 nm and mass concentration of $MoS_2$ powder (B). (ATP concentration was 1 mg $mL^{-1}$, ultrasonic time was 30 h.)

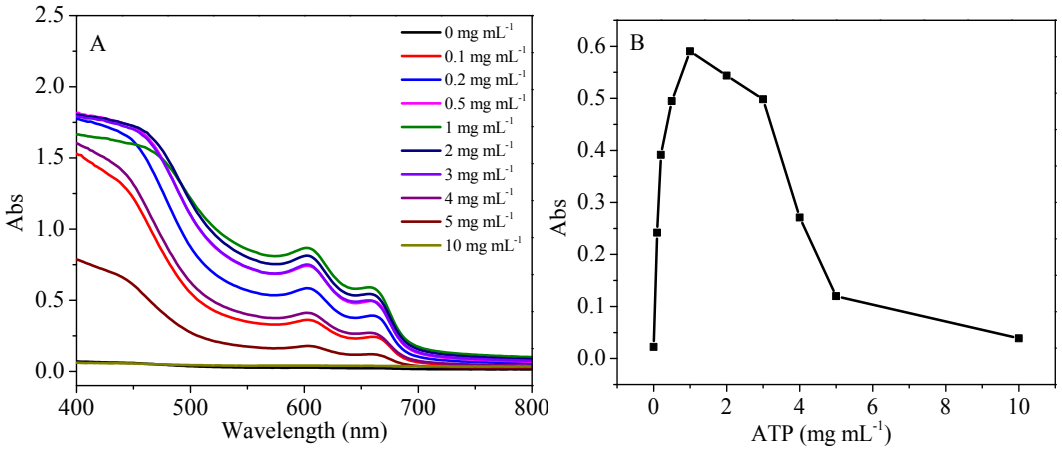


**Figure S8.** Absorption spectra of as-exfoliated $MoS_2$ nanosheets with different concentrations of ATP (A) and the relationship between absorption intensity of as-exfoliated $MoS_2$ nanosheets at 658 nm and ATP concentration. (B) ($MoS_2$ mass was 5 mg $mL^{-1}$, ultrasonic time was 30 h.)

**Table S1.** Comparison of exfoliation yield of $MoS_2$ nanosheets by direct ultrasonication in solvent

| Solvent | Time | Yield | References |
|---|---|---|---|
| N-methyl-pyrrolidone | 140 h | 40% | S3 |
| Ethanol/water | 8 h | 0.6% | S4 |
| Ethanol | 48 h | 21% | S5 |
| Water | 48 | 6% | S5 |
| Chloroform/acetonitrile | 1 h | 13.3% | S6 |
| Water | 30 h | 2.3% | This work |

**Table S2.** Comparison of aqueous ultrasonic exfoliation of TMDCs with the assistant reagents

| Assistant reagents | Time | Yield | Application | References |
|---|---|---|---|---|
| High-molecular weight ssDNA | 3 h | 80%-90% ($WS_2$/$WSe_2$) | antibacterial application | S7 |
| Alkali lignin | 80 h | 17.5% ($MoS_2$) | lithium ion battery | S8 |
| Nanocellulose | 4 h | 18% ($MoS_2$) | sodium ion battery | S9 |
| Chitosan | 5 h | 25.5% ($MoS_2$) | composites | S10 |
| Sodium cholate | 16 h | 10% ($MoS_2$) | lithium ion batteries | S11 |
| Bovine serum albumin | 35 h | 27.2 % ($MoS_2$) | adsorption and capacitance | S12 |
| Gelatin | 8 h | 1.6% ($MoS_2$) | composites | S13 |
| Gelatin | 8 h | 1.8% ($MoS_2$) | composites | S13 |
| Chitin nanofibrils | 48 h | 13.2% ($WS_2$) | supercapacitors and photo-thermal converter | S14 |
| Thermoresponsive polymeric ionic liquid | 18 h | 24.8% ($MoS_2$) | highly thermally conductive films | S15 |
| Tannic acid | 2 h | 60.5% ($MoS_2$) | photothermal nanocarriers | S16 |
| Nafion | 8 h | 8.8% ($MoS_2$) | memory membrane | S17 |
| Poly(3,4-ethylenedioxythiophene ):poly(styrenesulfonate) | 50 h | 1.6% ($MoS_2$) | organic solar cells | S18 |
| Bovine serum albumin | 10 | 15.4% ($WSe_2$) | photodynamic/photothermal therapy | S19 |
| ATP | 30 h | 23.6% ($MoS_2$) | biosensor | This work |

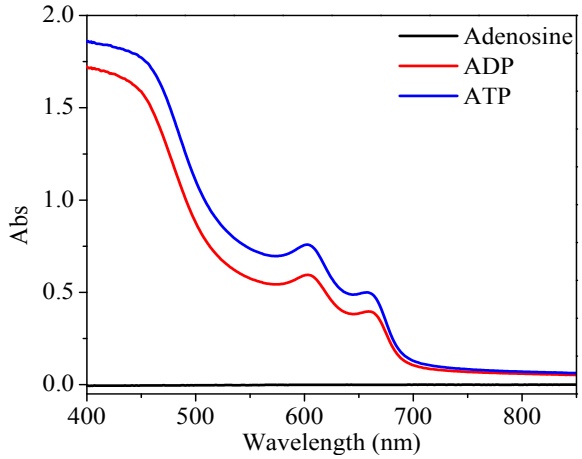


**Figure S9.** Absorption spectra of dispersion solutions of as-exfoliated $MoS_2$ nanosheets obtained from ultrasonic exfoliation with adenosine, ADP and ATP as the exfoliation reagent, respectively. 200 mg $MoS_2$ powder was added into 40 mL aqueous solution containing 40 mg ATP, ADP or adenosine, respectively and was ultrasonically exfoliated for 30 h.

**Theoretical calculation of $MoS_2$-ATP**

To study the adsorption of ATP on $MoS_2$ nanosheets, first-principles calculations based on density functional theory (DFT) were carried out by using the Vienna ab initio simulation package[S1] (VASP) with the projected augmented wave (PAW) method. The generalized gradient approximation Perdew-Burke-Ernzerhof (PBE) exchange-correlation functions were employed. For the calculations of binding energy, the first Brillouin zone was sampled with a 1×1×1 Monkhorst-Pack grid. All the structures were fully relaxed with residual forces smaller than 0.5 eV/Å. In addition, effect of vdW interaction was accounted for by using the dispersion corrected DFT (vdW-DF2 functional).[S2] The vacuum length was longer than 20 Å to decouple interaction between adjacent layers. The adsorption energy (*E(a)*) of ATP molecule on defective $MoS_2$ layer was calculated as $E(a) = E(MoS_x\text{-}molecule) - E(MoS_x) - E(molecule)$, where E(molecule), $E(MoS_x)$, and $E(MoS_x\text{-molecule})$ were the energies of ATP molecule, the defective $MoS_2$ layer, and the complex of defective $MoS_2$ and ATP molecule, respectively. In this work, the defective $MoS_2$ monolayer was constructed by S-Mo-S three atom layers with a large rhombohedral supercell that contains 81 Mo and 161 S atoms. On a side of S layers, one S atom was defected (see Figure S10 (a)). To simulate the ATP-doped $MoS_2$ synthesized experimentally, an ATP molecule was introduced in the above supercell, and terminal O atom of terminal phosphate in the ATP was set in the S defect in the $MoS_2$ monolayer, the corresponding stoichiometry was $Mo_{161}S_{81}C_{10}H_{16}N_5O_{13}P_3$ (see Figure S10 (b-c)).

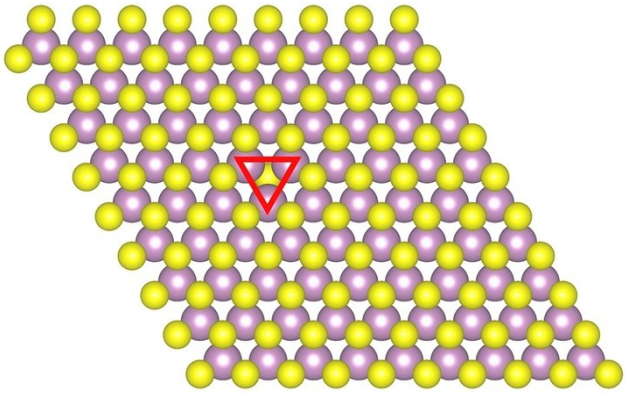

(a)

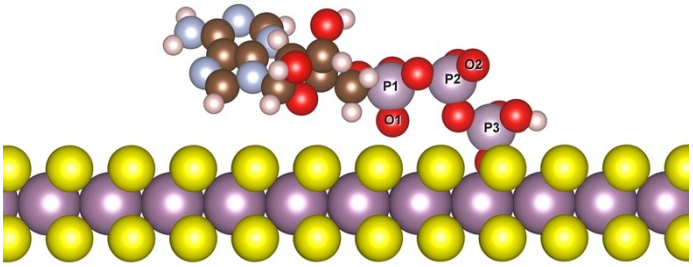


(b)

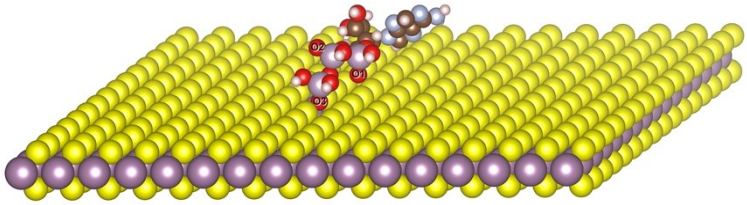

(c)

**Figure S10.** The top views of defective $MoS_2$ (a) and the side views (b) (c) of ATP on the defective $MoS_2$ monolayer

**Results of theoretical calculations**

To study the adsorption of ATP on $MoS_2$ nanosheets, we simulated the adsorption energy of ATP molecule on $MoS_2$ monolayer by using the density of function (DFT). The results of structural optimizations show that ATP molecule can be attached to $MoS_2$ monolayer through the formation of three Mo-O bonds (one strong binding within 2.40 Å bond length and two vdW binding with 2.85 and 2.89 Å). The adsorption energy of ATP on $MoS_2$ monolayer is -0.34 eV. Namely, it shows that ATP molecule can stably adsorb on the defect $MoS_2$ nanosheets, which are agreement with experiment. As displayed in Figure S10, it is clear that the terminal O atom of terminal phosphate in the ATP molecule tends to take up the S defect position, then bonds to Mo atoms. After adsorption, the double bond of P-O is broken. The length of new formed P-O bond is about 1.50 Å, 0.04 Å larger than the former double bond. Besides, two other terminal O atoms in the ATP molecule behave different. One has no changes due to far from S atoms layer after adsorbing and the other is repelled by S atoms layer, which results from perpendicularly closer to S atoms layer after

adsorbing. This can be proved by the bond lengths of P-O in Table S2. Thus, it shows that ATP will be easy to adsorb on the S atomic vacancy defect of $MoS_2$ monolayer, and it may be hard to adsorb in the pure $MoS_2$ monolayer.

**Table S3** The bond length of P-O in the ATP molecule.

| Bond length (Å) | P1-O1 | P2-O2 | P3-O3 |
|---|---|---|---|
| ATP molecule | 1.47 | 1.46 | 1.46 |
| ATP on $MoS_2$ monolayer | 1.40 | 1.46 | 1.50 |

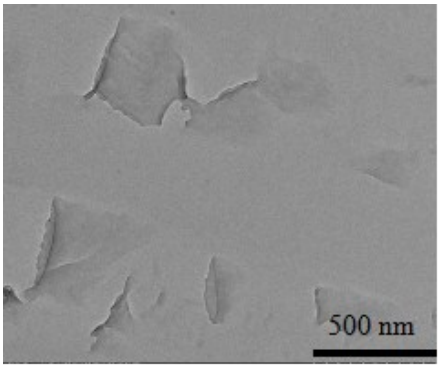


**Figure S11.** TEM image of as-exfoliated $WS_2$ nanosheets

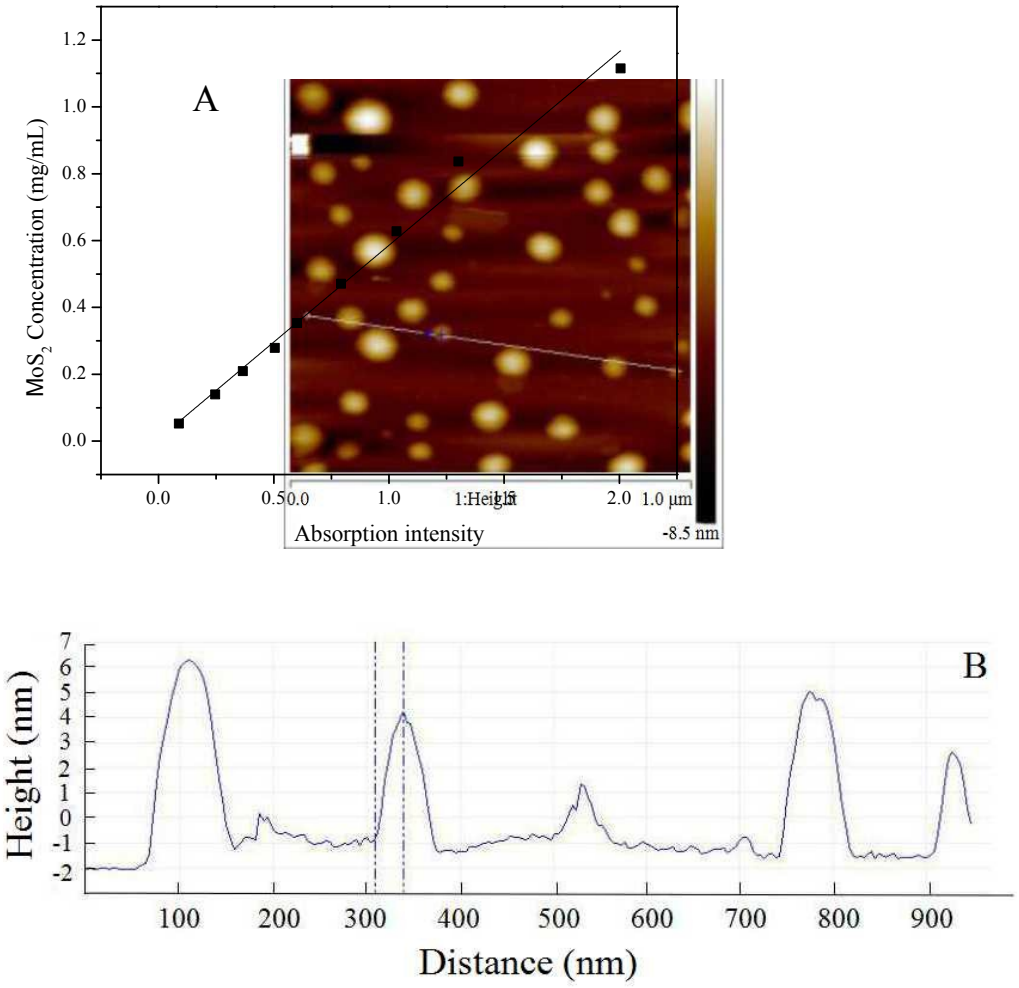


**Figure S12.** AFM image (A) and height profile (B) of the as-exfoliated $WS_2$ nanosheets

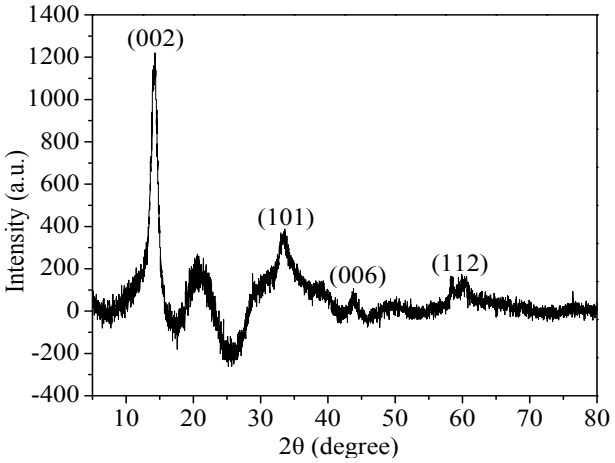


**Figure S13.** XRD image of as-exfoliated $WS_2$ nanosheets

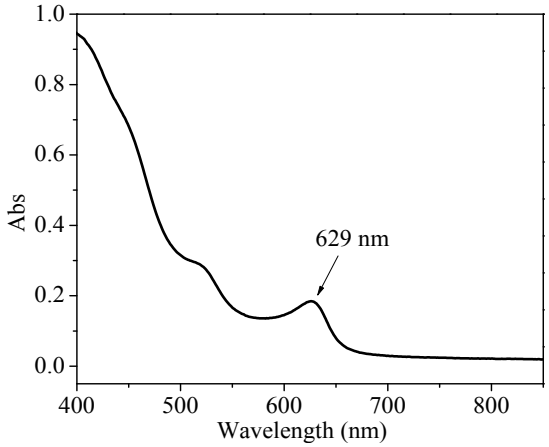


**Figure S14.** Absorption spectrum of as-exfoliated $WS_2$ nanosheets dispersion

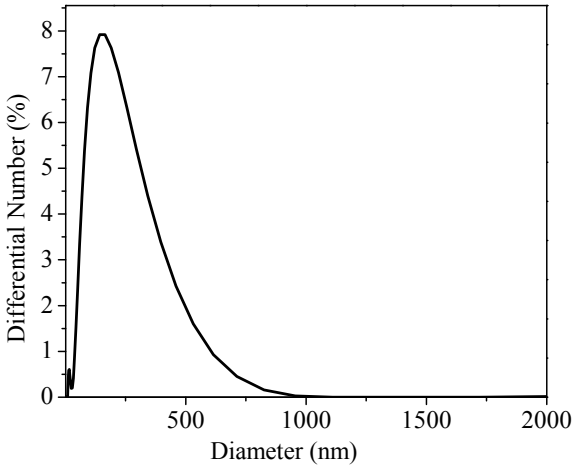


**Figure S15.** The size distribution of as-exfoliated $WS_2$ nanosheets

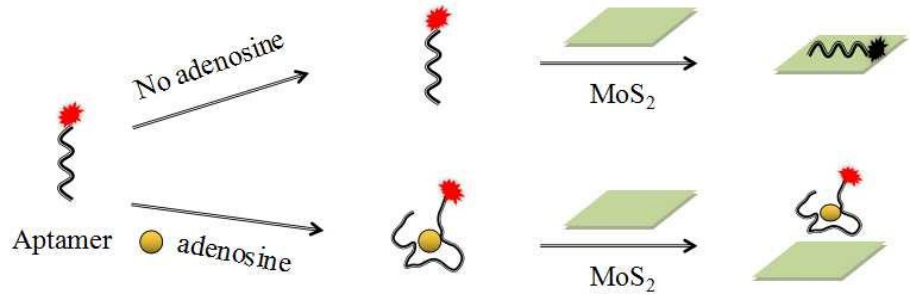


**Scheme S1.** The fluorescent biosensor for adenosine based on as-exfoliated $MoS_2$ nanosheets as the quenching platform.

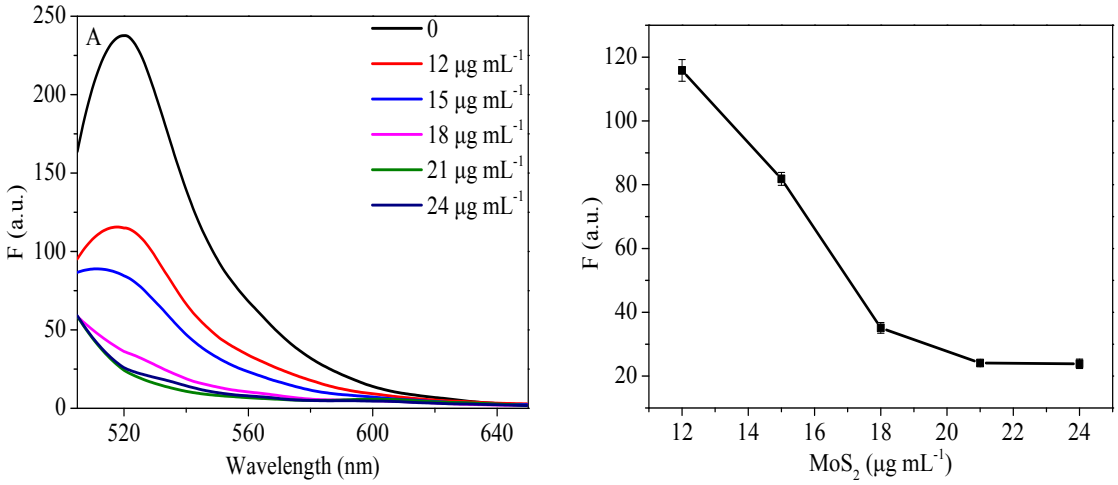


**Figure S16.** Fluorescence spectra (A) of FAM-labelled anti-adenosine aptamer (100 nmol $L^{-1}$) in the presence of different concentrations of as-exfoliated $MoS_2$ nanosheets; (B) Effect of as-exfoliated $MoS_2$ nanosheets concentration on the fluorescence intensity of FAM-labelled anti-adenosine aptamer. Excitation and emission wavelengths were 495 and 520 nm, respectively.

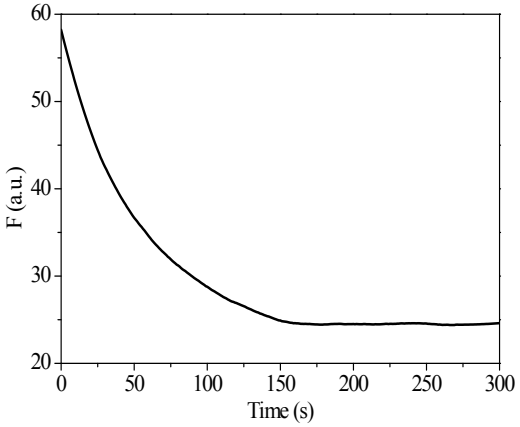


**Figure S17.** Fluorescence kinetic curve of FAM-labelled anti-adenosine aptamer (100 nmol $L^{-1}$) on addition of 21 μg $mL^{-1}$ as-exfoliated $MoS_2$ nanosheets. Excitation and emission wavelengths were 495 nm and 520 nm, respectively.

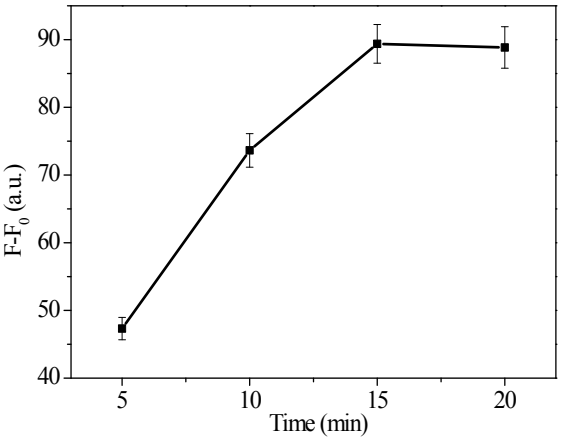


**Figure S18.** Effect of incubation time on the fluorescent enhancement upon addition of 1 mmol $L^{-1}$ adenosine into the mixtiure of 100 nmol $L^{-1}$ FAM-labelled anti-adenosine aptamer with 21 μg $mL^{-1}$ as-exfoliated $MoS_2$ nanosheets. Excitation and emission wavelengths were 495 nm and 520 nm, respectively.

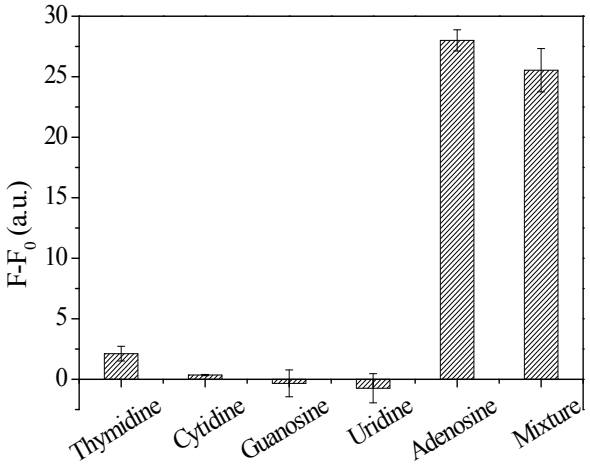


**Figure S19.** The fluorescent enhancement of this biosensor on addition of 50 μmol $L^{-1}$ adenosine, 250 μmol $L^{-1}$ thymidine, 250 μmol $L^{-1}$ cytidine, 250 μmol $L^{-1}$ guanosine, 250 μmol $L^{-1}$ uridine, and the mixture of 50 μmol $L^{-1}$ thymidine, 50 μmol $L^{-1}$ cytidine, 50 μmol $L^{-1}$ guanosine, 50 μmol $L^{-1}$ uridine, and 50 μmol $L^{-1}$ adenosine.

**Table S4.** Recoveries for the detection of spiked adenosine in human serum samples

| Samples | Added (μmol $L^{-1}$) | Found mean ± SD (μmol $L^{-1}$, n=3) | Recovery (%) |
|---|---|---|---|
| 1 | 10.0 | 8.6 ± 2.6 | 86.0 |
| 2 | 25.0 | 24.3 ± 7.2 | 97.2 |
| 3 | 40.0 | 36.8 ± 5.9 | 92.0 |

**References**


[S1] G. Kresse and J. Furthmüller, *Physical review B*, 1996, **54**, 11169.

[S2] K. Lee, É. Murray, L. Kong, B. Lundqvist and D. Langreth, *Physical Review B*, 2010, **82**, 081101.

[S3] A. O'neill, U. Khan and J. N. Coleman, *Chemistry of Materials*, 2012, **24**, 2414.

[S4] K. G. Zhou, N. N. Mao, H. X. Wang, Y. Peng and H. L. Zhang, *Angewandte Chemie International Edition*, 2011, **50**, 10839.

[S5] X. Hai, K. Chang, H. Pang, M. Li, P. Li, H. Liu, L. Shi and J. Ye, *Journal of the American Chemical Society,* 2016, **138**, 14962.

[S6] S. L. Zhang, H. Jung, J. S. Huh, J. B. Yu and W. C. Yang, *Journal of Nanoscience and Nanotechnology,* 2014, **14**, 8518.

[S7] G. S. Bang, S. Cho, N. Son, G. W. Shim, B. K. Cho and S. Y. Choi, *ACS Applied Materials & Interfaces,* 2016, **8**, 1943.

[S8] W. Liu, C. Zhao, R. Zhou, D. Zhou, Z. Liu and X. Lu, *Nanoscale,* 2015, **7**, 9919.

[S9] Y. Li, H. Zhu, F. Shen, J. Wan, S. Lacey, Z. Fang, H. Dai and L. Hu, *Nano Energy,* 2015, **13**, 346.

[S10] X. Feng, X. Wang, W. Xing, K. Zhou, L. Song and Y. Hu, *Composites Science and Technology,* 2014, **93**, 76.

[S11] R.J. Smith, P. J. King, M. Lotya, C. Wirtz, U. Khan, S. De, A. O'Neill, G. S. Duesberg, J. C. Grunlan, G. Moriarty and J. Chen, *Advanced Materials*, 2011, **23**, 3944.

[S12] G. Guan, S. Zhang, S. Liu, Y. Cai, M. Low, C. P. Teng, I. Y. Phang, Y. Cheng, K. L. Duei, B. M. Srinivasan and Y. Zheng, *Journal of the American Chemical Society*, 2015, **137**, 6152.

[S13] Yu Ge, Jialiang Wang, Zixing Shi, Jie Yin, *Journal of Materials Chemistry*, 2012, 22, 17619.

[S14] J. You, L. Zhu, Z. Wang, L. Zong, M. Li, X. Wu, and C. Li, *Chemical Engineering Journal*, 2018, **344**, 498.

[S15] X. Wang and P. Wu, *ACS Applied Materials & Interfaces*, 2018, **10**, 2504.

[S16] C. Zhang, D. F. Hu, J. W. Xu, M. Q. Ma, H. Xing, K. Yao, J. Ji and Z. K. Xu,

*ACS Nano*, 2018, **12**, 12347-12356.

[S17] W. Jia, B. Tang and P. Wu, *Nano Research*, 2018, **11**, 542.

[S18] W. Xing, Y. Chen, X. Wu, X. Xu, P. Ye, T. Zhu, Q. Guo, L. Yang, W. Li and H. Huang, *Advanced Functional Materials*, 2017, 27, 1701622.

[19] X. Jia, J. Bai, Z. Ma, X. Jiang,, *Journal of Materials Chemistry B*, 2017, 5, 269.